Space Charge Effects on Relative Peak Heights in Fourier Transform-Ion Cyclotron Resonance Spectra

Guy T. Uechi and Robert C. Dunbar
Chemistry Department, Case Western Reserve University, Cleveland, Ohio, USA

Ion trajectory calculations have confirmed that space charge interactions can be a source for mass discrimination seen in Fourier transform-ion cyclotron resonance (FT-ICR) spectra. As compared with the previously recognized mechanism of z-axis excitation, ion-ion repulsion is a mechanism which specifically affects relative peak heights of ions close in mass, and is most severe for low excitation radiofrequency (rf) amplitudes. In this mechanism, Coulomb repulsion significantly perturbs the motion of the ion clouds during excitation and alters the final cyclotron orbital radii. Under these conditions peak heights do not accurately reflect the true ion abundances in the FT-ICR spectrometer. Mass discrimination can be minimized by using low numbers of ions, low ion densities, and a short, high amplitude rf excitation waveform. Experimental observation of the relative peak heights of the m/z 91, 92, and 134 ions in *n*-butylbenzene gives quantitative confirmation of the results of the trajectory calculations. Chirp, SWIFT, and impulse excitation were modeled: impulse excitation was found to be most effective in minimizing the effects of space charge interactions. *(J Am Soc Mass Spectrom 1992, 3, 734–741)*

It is well known that the relative peak heights in Fourier transform-ion cyclotron resonance (FT-ICR) spectra do not always reflect accurately the ratios of ion abundances [1]. For ions far apart in mass, incorrect peak height ratios have been convincingly ascribed to selective z-axis ejection artifacts [2–6]. However, peak height ratios can also show large inaccuracies for ions close in mass, for which this mechanism is insignificant. The interaction of ions through their Coulomb repulsion, often referred to as space charge interaction, provides an alternative mechanism for distorting the relative intensities of FT-ICR spectra. We describe here experimental results and computer simulations which indicate that space charge interactions account for the inaccurate ratios of close-lying mass doublets. Wang and Marshall [7] have described analogous calculations and experiments examining the space charge interaction and the resulting minor peak broadening for ions of the same mass; the present consideration of the intensity ratios for mass doublets represents quite a different situation.

Experimental

The m/z 91 to 92 branching ratios and other experimental results were obtained on a homebuilt FT-ICR spectrometer. The ICR instrument contains a 2.5 cm cubical cell in a magnetic field of 1.4 Tesla, controlled by an IonSpec FT-ICR data system. At an indicated pressure of 3×10^{-8} torr, ions were produced by the electron impact fragmentation of *n*-butylbenzene at a nominal electron energy of 15 eV. Typical emission currents were 0.05–0.10 μA. Ions were trapped for 100–250 ms at a trapping plate voltage of 4 V (except where noted otherwise).

The radiofrequency (rf) amplitude was measured peak to peak at the transmitter plates. Peak heights were used to obtain the branching ratio rather than peak areas. The widths of the peaks (full width half-maximum) were observed to be the same, so the question of whether to measure peak heights or areas was not significant.

Results

Figure 1 shows measurements of the 91/92 peak height ratio (fragment ions of *n*-butylbenzene) as a function of rf excitation amplitude, using chirp excitation. Concurrent measurements using impulse excitation, low ion number, and low trapping voltage, conditions which were expected to approach closely to an accurate ratio measurement, gave a ratio of 1.0, which was taken to be the true ratio for these ionizing conditions. (Our confidence that this latter measurement gave true ratios was reinforced by a similar measurement of the

Address reprint requests to Robert C. Dunbar, Chemistry Department, Case Western Reserve University, Cleveland, OH 44106

1044–0305/92/$5.00

Received September 23, 1991
Revised April 20, 1992
Accepted May 4, 1992

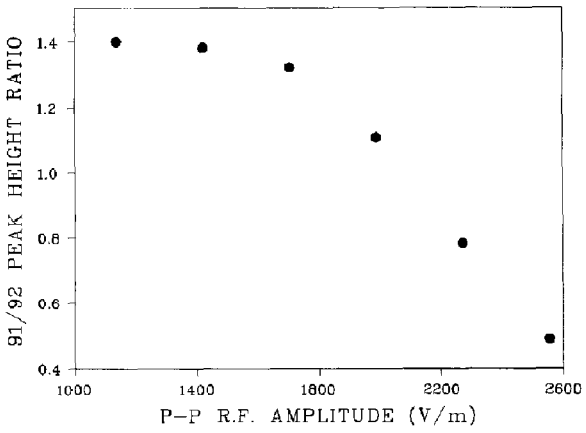

Figure 1. Experimentally obtained peak height ratio of m/z 91 and 92 as a function of chirp excitation amplitude.

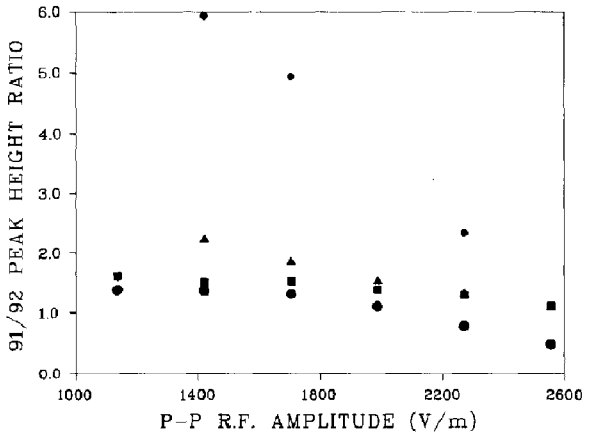

Figure 2. Experimental peak height ratio of m/z 91 to 92, similar to Figure 1, with the number of ions in the trap controlled by using various lengths of the electron beam pulse: 5 ms (•); 10 ms (■); 25 ms (▲); 100 ms (•).

bromine 79/81 isotope ratio in bromobenzene ions as 1.02, which is correct.)

It is seen that at low rf amplitudes the observed 91/92 ratio is substantially too high (about 1.4), while at high rf amplitudes it drops sharply below 1.0. We ascribe the dropoff in ratio at excitation amplitudes above 2000 V/m to preferential cyclotron ejection of m/z 91 ions. However, below 2000 V/m there is no reason to expect cyclotron ejection of ions of either mass, and we attribute the increase in ratio from 1.0 to 1.4 to ion-ion Coulomb repulsion ("space charge effects"). The conditions resulting in the ratios shown in Figure 1 were taken as the basis for comparison with the computer simulations of space charge effects described below, and a goal of the simulations was to see if reasonable parameter choices would lead to a good match with this set of experimental results.

If we postulate that space charge repulsions are the cause of the inaccurate peak ratios of close mass doublets, there are various predictions that can be experimentally tested: this model predicts that the ratio should become more accurate as the ion-ion repulsions are reduced by (1) reducing the number of ions in the trap, (2) reducing the trapping voltage to give a shallower, broader trapping well along the z direction, and (3) increasing the excitation amplitude. Some limited experiments were done to test these predictions. Figure 2 shows the effect of increasing the number of ions by increasing the electron beam pulse length. (The lowest value, 5 ms, corresponds to the data of Figure 1.) It is seen that the ratios generally move farther above the correct value of 1.0 as the number of ions increases, for any given rf excitation amplitude. The longest beam pulse (100 ms) combined with a low rf level (1420 V/m) gave an extreme mass discrimination of about a factor of 6.

It was found hard to do convincing experiments varying the trapping potential, because this gave variations in ion trapping and detection conditions which were not easily standardized. It was observed, however, that increasing the trapping voltage from 1.5 to 3.5 V gave a large increase in the observed bromine isotope ratio for bromobenzene ions (an increase of as much as a factor of 3 at low rf amplitude).

Finally, as is clear in Figures 1 and 2, low rf excitation amplitudes gave the greatest mass discrimination. At the lowest rf levels, where the signal was approaching the noise level, mass discrimination was typically very severe.

Computer Modeling

Convincing support for the space charge mechanism of mass discrimination for close-lying peaks can be gained through computer simulation of the experiments. The goal is to show that Coulomb repulsion, by using physically reasonable parameter values, does actually lead to mass discrimination in the observed direction, with the right magnitude, and having the correct dependences on ion density and rf level. Accordingly, we undertook extensive computer simulations of these effects, and the success of these simulations provides the strongest indication we can give for the relevance of the Coulomb repulsion model of mass discrimination.

The effect of Coulomb interactions during excitation was modeled for the system consisting of two ion clouds (masses 91 and 92). The trajectory of each ion cloud was calculated by numerical integration of Newton's second law for motion of an ion experiencing the repulsion of a charge cloud at relative position r.

$$\mathbf{F} = \mathbf{ma} = q\mathbf{E} + (\mathbf{qv}/\mathbf{cxB}) + (1/4\pi\epsilon_0)qq_2\mathbf{r}/|\mathbf{r}|^3 \quad (1)$$

where F is the force on an ion of mass m and charge q, E (volts/m) is the instantaneous electric field along the

x axis, **v** (m/s) is the velocity, **B** (Tesla) is the magnetic field along the z axis, and q_2 is the charge of the repelling ion cloud. The cyclotron motion of the ion is in the x-y plane because the direction of the magnetic field is along the z axis. Each of the two ion clouds was represented as a single point having the charge of the total number of ions in the cloud.

Two assumptions were made in the model to simplify the calculations. First, the initial thermal velocity of the ions was neglected. The contribution of the thermal velocity of the ions to the overall signal is essentially zero. The direction of the thermal velocity of each ion is random, so that the net velocity vector of all the ions in the ion cloud is zero. A signal induced on the receiver plates of the ICR cell can only be produced by the coherent motion of a packet of ions in a cyclotron orbit. While the random thermal motion of the ions thus makes no direct contribution to the signal, it may affect the ion trapping and the signal strength through various mechanisms involving ion-ion collisions, coupling of z-axis and cyclotron motions, and other nonlinear terms in the equation of motion [2]. We did not see that these possibilities would be important in the present context, and did not try to include them in the modeling.

Second, a simplified picture was adopted to model the distribution of ions along the z axis and in the x-y plane. The initial relative position of the interacting ions has a significant effect on the role of Coulomb repulsion in the ion trajectories. Table 1 shows calculated final cyclotron radii for ion pairs having five different initial orientations, giving somewhat varying Coulomb contributions to the mass discrimination. An average over these five orientations gives a result quite similar to that obtained for the single case of ions both lying along the z axis. Taking this to be a generally good approximation, the calculations were simplified by positioning the two ion clouds initially along the z axis in all further simulations.

The numerical integration was carried out by straightforward iteration of the different equations corresponding to eq 1

$$x_1^{i+2} = 2x_1^{i+1} - x_1^i + \frac{q_1 E_x}{m_1}\Delta t^2 + \frac{q_1 \mathbf{B}}{m_1}(y_1^{i+1} - y_1^i)\Delta t - \frac{q_1 q_2}{4\pi\varepsilon_o m_1}\frac{(x_2^{i+1} - x_1^{i+1})}{R^3} \quad (2)$$

$$y_1^{i+2} = 2y_1^{i+1} - y_1^i - \frac{q_1 \mathbf{B}}{m_1}(x_1^{i+1} - x_1^i)\Delta t - \frac{q_1 q_2}{4\pi\varepsilon_o m_1}\frac{y_2^{i+1} - y_1^{i+1}}{R^3} \quad (3)$$

and a similar pair of equations with labels 1 and 2 interchanged. Here x_1^i, x_1^{i+1}, and x_2^{i+2} give the position of ion 1 after zero, one and two time steps (with similar notation for the y coordinate), q_1 is the charge of ion 1, q_2 is the total charge of ion cloud 2, m_1 is the mass of ion 1, R is the distance between ion 1 and ion cloud 2, and Δt is the time step for the integration.

Table 1. Ratios of *m/z* 91 and 92 final cyclotron radii calculated by using different initial ion positions[a]

Initial Position of *m/z* 92 (mm)	Calculated 91 radius /92 radius (mm /mm)
(0, 0, .15)	8.27 /6.23 = 1.32
(.15, 0, 0)	8.54 /6.27 = 1.36
(-.15, 0, 0)	7.96 /6.37 = 1.25
(0, .15, 0)	8.62 /6.23 = 1.38
(0, -.15, 0)	8.26 /6.33 = 1.30
	average = 1.32 ± 0.01

[a] 50 V rf amplitude, 0.20 ms chirp excitation *m/z* 95–88, 5000 ions in each cloud. *m/z* 91 is placed at (0, 0, 0).

Some attention was necessary in the choice of the time step Δt. If Δt was chosen too large, accumulated errors in the numerical integration resulted in gradually increasing ion orbits in the absence of any electric force. Δt was empirically chosen to limit the drift of the orbiting radii to less than 0.5% with each successive cycle. This criterion was comfortably satisfied at a Δt value (1.1 ns) which give a complete cyclotron orbit for an ion of mass 91.5 in 4000 time steps. Inspection of ion motion plots like those shown below indicated that this time step was satisfactorily short even during the initial period of rapid ion acceleration under the influence of Coulomb repulsion.

Excitation Schemes

Three excitation schemes were modeled to compare the effect of the Coulomb interaction on the peak ratio:

1. Chirp (frequency sweep) excitation [8, 9]:

$$E(\text{chirp})_x = E_o(0.72/2.54 \times 10^{-2}\text{m})\sin(\omega_i t + 0.5at^2) \quad (4)$$

where E_o is the amplitude of the rf voltage applied to the receiver plates, 0.72 is a correction factor to the potential in a cubic cell [10], 2.54×10^{-2} m is the length of a side of the cubical cell, ω_i is the starting frequency in radians/s, t is time in seconds, and a is the sweep rate in radians/s^2. The parameters were chosen to match the experimental conditions corresponding to Figure 1, with a mass range from 95 to 88 swept in 200 μs.

2. Impulse excitation [11, 12]. This was modeled as a constant electric field turned on for 1 μs in the x direction.

$$E(\text{impulse})_x = E_o(0.72/2.54 \times 10^{-2}\text{m}) \quad 0 < t < 1\ \mu\text{s} \quad (5)$$

3. SWIFT excitation [13, 14]. SWIFT is not actually a specifically defined excitation waveform, but describes a family of waveforms having the desired excitation spectrum. In the preferred implementation, the phases of the Fourier components are scrambled in such a way that the excitation rf amplitude is spread out reasonably uniformly over the duration of the excite pulse. This was mimicked by the sum of two sinusoidal waveforms at the specific frequencies for m/z 91 and 92:

$$E(SWIFT)_x = E_o(0.72/2.54 \times 10^{-2}m) \{\sin \omega_{91}t + \cos \omega_{92}t\} \quad (6)$$

which accelerated the ion clouds for 200 μs.

Computer Modeling Results

The first set of calculations investigated whether the inclusion of the Coulombic term affected the trajectory of the ions in a way that would explain the mass discrimination seen in Figure 1. Figures 3 and 4 are sets of plots that show the trajectories of ion clouds m/z 91 and 92 with the absence and inclusion of the Coulomb repulsion term respectively. Each ion cloud contained the charge of 5000 ions and was accelerated by a chirp excitation waveform of amplitude E_o = 40V sweeping through m/z 95–88 in 200 μs. The separation of the ion clouds was 0.125 mm along the z axis.

The inclusion of Coulomb repulsion between the two ion clouds clearly has a direct effect on the final cyclotron orbital radius after chirp excitation. FT-ICR peak heights are expected to be proportional to the final cyclotron radii of the two ion clouds after excitation [15]. The difference in the calculated cyclotron radii is large enough to account for the mass discrimination seen in the peak ratios for the set of data shown in Figure 1. Table 2 shows the calculated dependence of the final cyclotron orbital radii on the chirp excitation amplitude.

Excellent quantitative agreement between the experimentally determined peak heights (electron beam length 5 ms) and the calculated final cyclotron orbital radii is seen in Table 2. The ratios for each excitation amplitude correspond well up to E_o = 70 V. At E_o = 80 V the calculated cyclotron radius of 91 exceeds 12 mm. This matches the cyclotron radius at which the orbiting ion cloud would begin to collide with the walls of the cell. This is seen in the observed dropoff in the experimental signal strength near this amplitude. The calculation predicts that m/z 91 has a larger radius than m/z 92, which is in agreement with the observation that it is preferentially ejected at high rf amplitudes.

Table 3 shows the mass discrimination produced by using the three types of excitation schemes: chirp (eq 4), impulse (eq 5), and the simulated version of SWIFT excitation (eq 6). The ion clouds each contained the charge of 5000 ions with a z axis separation of 0.125 mm. It is seen that mass discrimination is most severe for chirp excitation, smaller but still significant for simulated SWIFT excitation, and smaller still for impulse excitation.

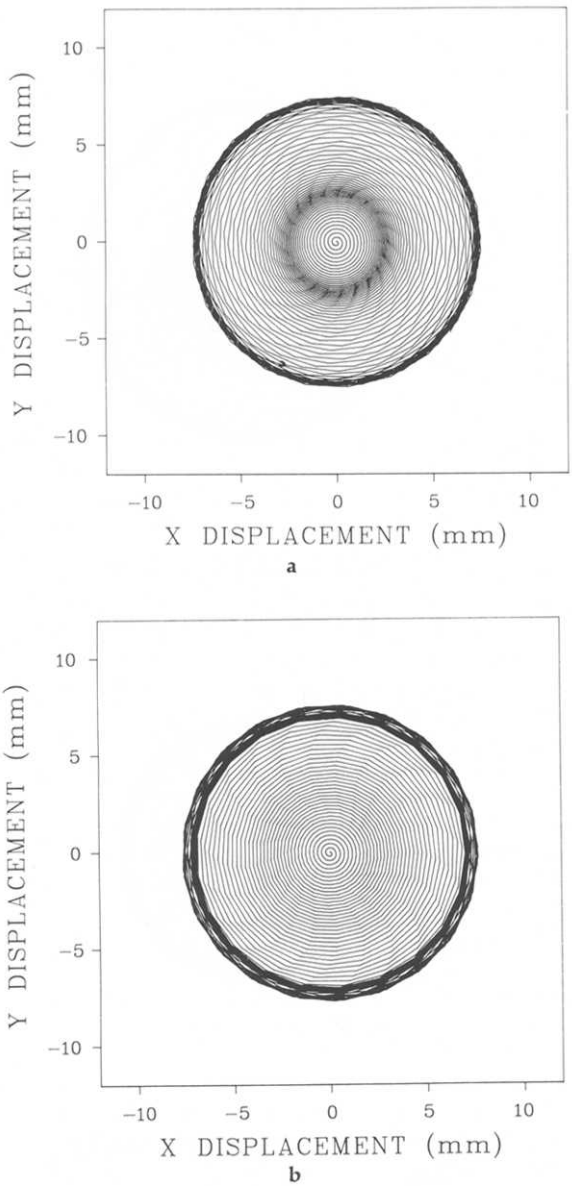

Figure 3. Trajectory plots of the ion clouds calculated in the model, without Coulomb interaction. (a) m/z 91; (b) m/z 92.

Further Modeling Studies

To probe further the modeled space charge effect a series of calculations was made to observe the response of the ratio of the final cyclotron orbital radii to changes in various parameters. Figure 5 compares the space charge effect for the close-lying 91/92 doublet and the

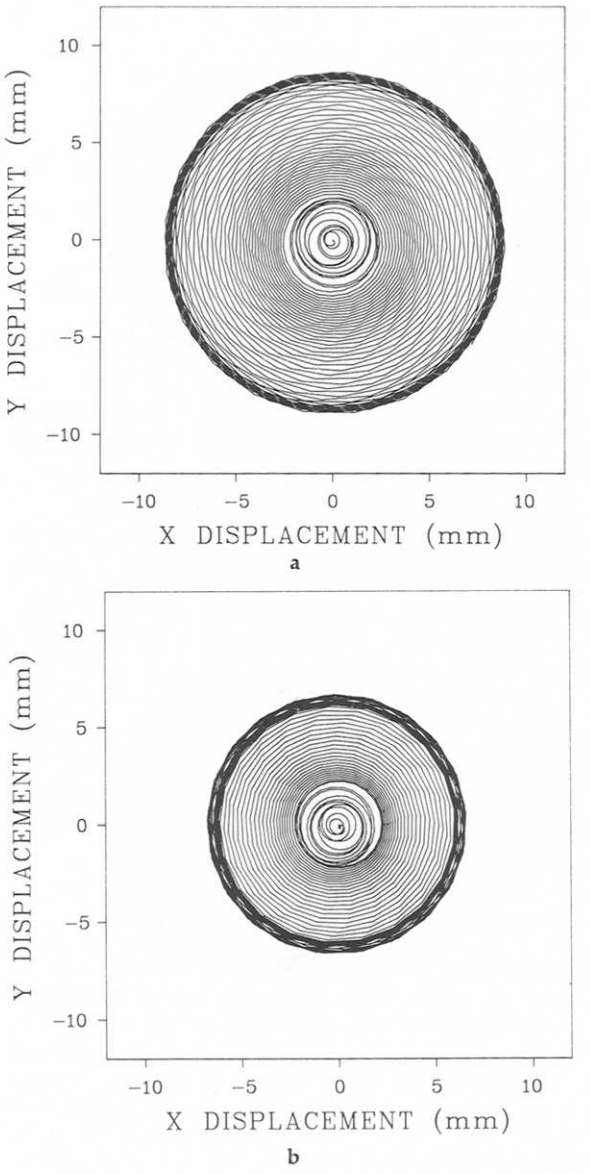

Figure 4. Plots identical to Figure 2 except Coulomb interaction between the ion clouds is included. (a) m/z 91; (b) m/z 92.

Table 2. Experimental peak ratios and calculated cyclotron orbital radii for m/z 91 and 92 as a function of rf amplitude (chirp excitation)

E_0(v)	Experimental 91 /92 (arbitrary units)	Calculated 91 radius /92 radius (mm /mm)
40	3.29 /2.35 = 1.40	6.78 /4.75 = 1.42
50	3.96 /3.08 = 1.38	8.52 /6.19 = 1.38
60	4.95 /3.48 = 1.32	9.42 /7.82 = 1.20
70	5.26 /4.74 = 1.11	10.59 /9.26 = 1.14
80	4.12 /5.27 = 0.78	12.55 /10.49 = 1.19
90	2.68 /5.48 = 0.49	13.55 /12.22 = 1.10

Table 3. The effect of Coulomb repulsion on calculated cyclotron orbital radii using three different excitation schemes

Excitation scheme	E_0	Pulse width	Calculated 91 /92 Coulomb off (mm /mm)	Calculated 91 /92 Coulomb on (mm /mm)
Chirp m/z 95–88	50v	0.2ms	7.27 /705 = 1.03	8.52 /6.19 = 1.38
Simulated SWIFT	20v	0.2ms	7.27 /7.26 = 1.00	8.06 /7.93 = 1.11
Impulse	400v	0.001ms	7.44 /7.46 = 1.00	7.66 /7.24 = 1.06

widely mass separated 91/134 doublet. The ions were excited by identical chirp excitation waveforms of pulse length 200 μs sweeping through m/z 200–50. Each ion cloud contained the charge of 3000 ions with an initial separation of 0.15 mm along the z axis. The effect on the cyclotron orbital radii ratio of m/z 91/92 was very dependent on the number of ions, while the effect on the 92/134 ratio was small. (The discrimination of up to 1.07 in the 92/134 ratio was largely independent of the Coulomb interaction, and represents numerical errors in the simulation.)

Figure 6 probes the effect of a shortened (but higher amplitude) chirp excitation pulse length on the ratio of the final cyclotron orbital radii of the ion clouds of m/z 91 and 92. To compensate the shortened pulse length the excitation amplitude was correspondingly increased to keep the final cyclotron radius of the ion clouds relatively constant at 7 mm in each run. Once again a charge of 3000 ions was given to each ion cloud with an initial z axis separation of 0.15 mm. Chirp excitation was used, sweeping through m/z 95–88. As the length of the chirp waveform was shortened the mass discrimination between m/z 91 and 92 decreased.

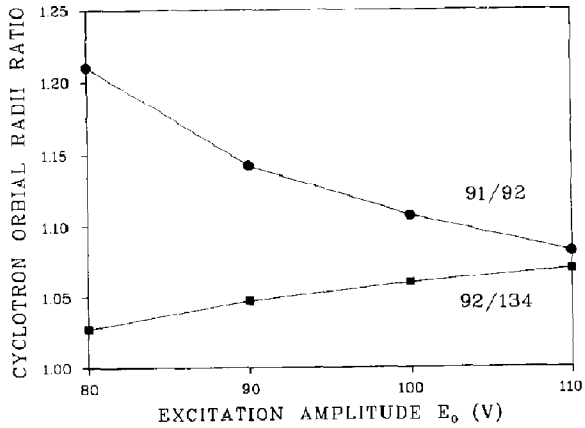

Figure 5. Ratio of the calculated cyclotron orbital radii as a function of rf excitation amplitude. (■) ratio of cyclotron radii for m/z 92 and 134; (●) ratio of cyclotron radii for m/z 91 and 92.

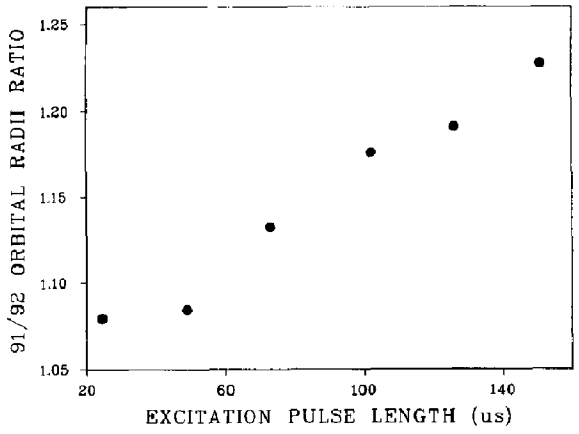

Figure 6. Ratio of the calculated cyclotron orbital radii of m/z 92 and 92 as a function of rf excitation pulse length. The excitation amplitude was lowered as the pulse length was lengthened to produce final cyclotron orbits of approximately 7 mm.

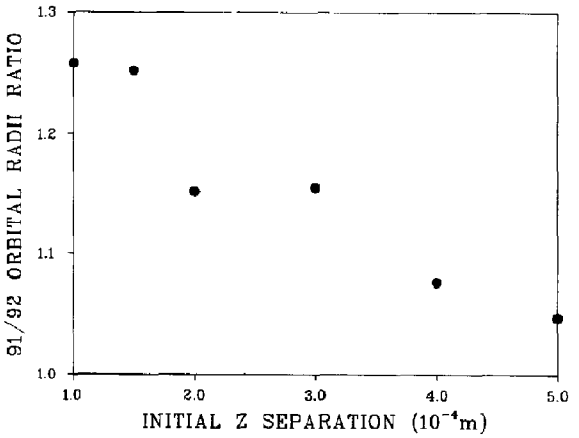

Figure 8. Ratio of calculated cyclotron orbital radii of m/z 91 and 92 as a function of initial separation of the ion clouds along the z axis.

The effect of reducing the total number of ions was modeled by decreasing the total charge in each ion cloud. Figure 7 shows the dependence of the 91/92 cyclotron orbital radius ratio on the rf excitation amplitude. Three cases were modeled: 3000 ions, 1500 ions, and 500 ions in each cloud. Chirp excitation of pulse length 200 μs swept through m/z 95–88, with an initial separation of the ion clouds of 0.15 mm along the z axis. Reduction in the total charge steadily reduced the extent of mass discrimination.

Lower ion densities were mimicked by increasing the initial z axis separation of ion clouds while keeping the total number of ions the same (as would be expected for a reducing trapping voltage). Each ion cloud contained the charge of 3000 ions, accelerated by a chirp excitation waveform sweeping through m/z 95–88 for 200 μs at E_o = 40 V. Figure 8 shows the lessening of the mass discrimination between m/z 91 and 92 as the ion clouds approach distances where the short range Coulomb interactions have little effect.

The simulations successfully modeled the qualitative increase in mass discrimination for increasing ion number, increasing trapping voltage, and decreasing excitation amplitude. However, the ion trajectories found in these simulations did not account quantitatively for the large mass discrimination seen at very high ion numbers and trapping voltages, as in the 100 ms data in Figure 2. This may reflect the limitation in modeling of the ion clouds as point charges.

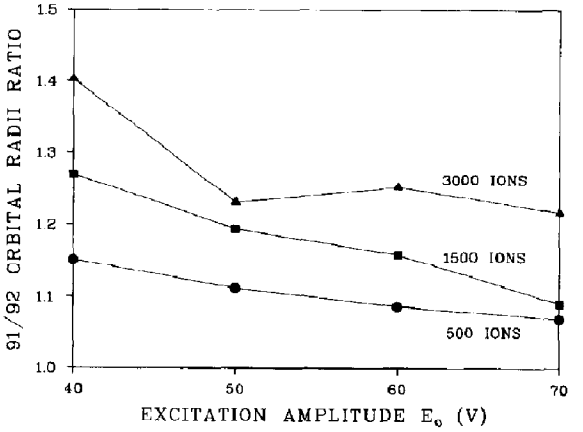

Figure 7. Ratio of calculated cyclotron orbital radii of m/z 91 and 92 as a function of rf excitation amplitude. (▲) 3000 ions in each cloud; (■) 1500 ions in each cloud; (●) 500 ions in each cloud.

Discussion

From the trajectory calculations we see that Coulomb repulsion significantly affects the motion of the ions during excitation. Figure 3 shows ion clouds, m/z 91 and 92, without Coulombic interaction, spiraling out from the center of the cell in a uniform manner as one would expect during excitation by an oscillating electric field. In Figure 4, the cyclotron motion during the chirp excitation is perturbed by the inclusion of Coulomb repulsion, resulting in altered final cyclotron orbits. Once the ion clouds have reached the final cyclotron orbital radii ion motion is unperturbed by Coulomb interactions.

The motion of the ion clouds during the chirp excitation is very complicated and it is not easy to interpret the simulation results. The relative phases of the ion clouds' cyclotron motions are not easily followed. Rather than attempt to understand in detail the interaction of the Coulomb force with the other forces during the excitation, we have focused on the space charge effects reflected in the calculated final cyclotron orbital radii. By using this criterion, the excellent agreement seen in Table 1 between simulated and observed space charge effects gives us confidence that we understand the mechanism of the 91/92 ratio dis-

tortion in an entirely satisfactory way, at least when the perturbation is relatively small.

The trajectory calculations have emphasized and clarified several features of the effect of space charge interactions on peak heights in FT-ICR spectra. First, mass discrimination by space charge effects is most important for ions close in mass. Second, the artifact can be minimized by using a short, high-amplitude excitation waveform. Both of these characteristics come naturally from the fact that the Coulomb perturbation of the ion motion depends on the length of time over which the interacting ions are close together during excitation. Third, the artifact is minimized by using low numbers of ions and by spreading the ions out along the z axis, both of which reduce the magnitude of the Coulomb forces.

Coulomb repulsion as a mechanism for mass discrimination is only significant for ions close in mass. Two ions of different mass that are initially traveling coherently in their cyclotron orbits will gradually fall out of phase, and move apart in space, due to their difference in cyclotron frequency. The cyclotron motions of ions far apart in mass dephase quickly. Ions at m/z 92 and 134 traveling with the same cyclotron orbital radius will be separated by one radian after about 2 μs, which is short compared with a typical chirp excitation pulse length of 200 μs. Once the ions have dephased in the first 2 μs of excitation, the short range Coulomb forces become negligible with respect to the force of the rf electric field. The dephasing period for ions m/z 91 and 92 is 62 μs, and the motion of ions is perturbed by Coulomb repulsion during a significant fraction of the excitation. The simulations clearly show this distinction between close-lying and far-apart mass doublets, as illustrated in Figure 5.

The length of the excitation waveform strongly determines the extent of mass discrimination. Figure 6 shows that as the chirp waveforms become shorter and higher in amplitude, the mass discrimination decreases. Once again the basic principle is that the length of time in which Coulomb repulsion significantly perturbs the motion of the ions determines the degree of mass discrimination. For a given extent of dephasing of the cyclotron motions of the interacting ions, the spatial separation between them is proportional to their cyclotron radii. If the excitation pulse length is shortened, the ions reach large cyclotron radii sooner, allowing dephasing to move them apart more quickly.

Impulse excitation uses a very short high-amplitude excitation waveform [11, 12]. Ideally, the length of the impulse excitation is chosen to be much less than one cycle of the cyclotron orbit of the ions in the ion trap cell. Impulse excitation in principle instantly increases the momentum of the ion cloud from rest producing all ions traveling in a large cyclotron orbit. At this large orbit a small angular separation due to dephasing will result in a large linear separation, minimizing Coulomb repulsion effects.

In obtaining accurate peak heights, SWIFT addresses the problem of the nonuniform frequency domain power spectrum produced by chirp excitation [9]. The ideal excitation scheme accelerates all the ions to the same cyclotron orbital radius. The amplitude of the image current produced on the receiver plates will then simply be proportional to the total number of ions in each ion cloud. The SWIFT excitation waveform is derived from the inverse FT of the desired frequency domain power spectrum [13, 14]. Various algorithms have now been developed for the production of the SWIFT waveform.

We did not attempt to produce an actual SWIFT waveform for the investigation but simply mimicked one. The sum of two sinusoidal waveforms which we used preserves the desired characteristics that the two ions are accelerated simultaneously, and the duration of the excitation is the same as the chirp waveform with which we are comparing.

Unfortunately, SWIFT will only remedy the problem of accurate peak heights to the extent that the mass discrimination artifact is produced by the nonuniform power spectrum of the excitation waveform. Even if the excitation waveform is designed to produce a flat power spectrum, the problem of Coulomb repulsion between ion clouds can still perturb the motion of the ions and mass discrimination may still persist. As Table 3 shows, the simulated SWIFT waveform we used gives less discrimination than the chirp, which seems to be particularly bad in this respect, but the SWIFT waveform by no means eliminates the discrimination. Moreover, for SWIFT pulses longer than the 200 μs we used, we would expect the discrimination to be more severe, following the arguments given above.

Mass discrimination due to ion repulsion can also be reduced by minimizing the magnitude of the Coulomb force existing between the two ion clouds. Experimentally, reducing the total number of ions and lowering the trapping potential both help to remedy the ion intensity ratio problem. Figure 7 shows that a reduced number of ions reduces the mass discrimination.

Lowering the trapping potential while keeping the number of ions the same reduces the ion density.[1] The lowered direct current voltage on the trapping plates produces a shallower potential well allowing the trapped ions to spread out along the z axis. The total number of ions will remain the same but at a lower ion density. This was modeled by keeping the total number of ions in each cloud the same while increasing the

[1] In considering that the ions are more compressed along the z axis at higher trapping voltage, we have assumed that the initial oscillations along the z axis have damped out, settling the ions to the center of the trap. It can be questioned whether z axis relaxation is complete in these low-pressure experiments; but we see substantial relaxation of the z axis motion judging from the increase and leveling off of the FT-ICR signal strength within a few hundred milliseconds after the electron beam pulse (see ref 2). The z axis relaxation is believed to be effected by Coulomb repulsions between ions along the z axis.

initial separation between ion clouds. Figure 8 shows the reduction in mass discrimination as the initial ion cloud separation increases.

Conclusions

Although FT-ICR spectrometry is an excellent means of studying ion chemistry, the problem of mass discrimination detracts from its strength as an analytical tool. Most of the problems with accurate peak ratios have been attributed to the motion of the ions during excitation.

The actual motion of ions in an FT-ICR spectrometer is complicated and can differ from the motion of a single ion in a cyclotron orbit. The experimental spectra are dependent on many variables that are sometimes hard to control. One of these variables is the space charge interaction among the ions in the ion trap. By using ion trajectory calculations we have studied the effects of interionic repulsion under various conditions. The effect of Coulomb repulsion on the final cyclotron orbital radius after excitation provides satisfactory understanding of the mass discrimination seen in spectra of close-mass ions. The trajectory calculations, reinforced by experimental observations, indicate that space charge effects can be minimized by (1) using low ion densities, (2) using low ion numbers, and (3) using an excitation scheme that accelerates the ions in a very short period of time. The first two criteria would favor the use of large cells, low trapping voltages, and small numbers of ions; even better should be cells elongated along the z direction [16], and cells with screened trapping plates [17], to spread the ions out along the z axis. The third criterion would suggest impulse excitation as the best excitation scheme for accurate peak ratios, with other excitation profiles being progressively worse as the acceleration period for the ions of interest grows longer.

Our finding of mass discrimination due to space charge effects and the remedies to the problem discussed here do not at all contradict or diminish previous work implicating z axis excitation and ejection of ions by the chirp waveform as the cause of large mass discrimination effects in ICR. Space charge provides another, additional source of FT-ICR peak ratio variations. In two respects the space-charge artifact contrasts with previously discussed mass discrimination mechanisms. First, it is most severe for ratios of ions lying closest together in mass, because of the slow dephasing of close-lying ions; and second, it is most severe at the lowest levels of rf excitation amplitude which maximize the ion-ion interaction time. The z axis mass discrimination effects are, by contrast, severe for ions lying far apart in mass and excited with large amplitude rf pulses [2].

Acknowledgments

The authors acknowledge the support of the National Science Foundation and of the donors of the Petroleum Research Fund, administered by the American Chemical Society; and the support of Guy T. Uechi by BP Research during the period of this work.

References

1. Moini, M.; Eyler, J. R. *Int. J. Mass Spectrom. Ion Processes* **1989**, *87*, 29–40.
2. Rempel, D. L.; Huang, S. K.; Gross, M. L. *Int. J. Mass Spectrom. Ion Processes* **1986**, *70*, 163–184.
3. Huang, S. K.; Rempel, D. L.; Gross, M. L. *Int. J. Mass Spectrom. Ion Processes* **1986**, *72*, 15–31.
4. Kofel, P.; Alleman, M.; Kellerhals, H. P.; Wanczek, K. P. *Int. J. Mass Spectrom. Ion Processes* **1986**, *74*, 1–12.
5. van der Hart, W. J.; van de Guchte, W. J. *Int. J. Mass Spectrom. Ion Processes* **1988**, *82*, 17–31.
6. Wang, M.; Marshall, A. G. *Anal. Chem.* **1990**, *62*, 515–520.
7. Wang, T. L.; Marshall, A. G. *Int. J. Mass Spectrom. Ion Proc.* **1986**, *68*, 287–301.
8. Comisarow, M. B.; Marshall, A. G. *Chem. Phys. Lett.* **1974**, *25*, 282–283.
9. Marshall, A. G.; Roe, D. C. *J. Chem. Phys.* **1980**, *73*, 1581–1590.
10. Dunbar, R. C. *Int. J. Mass Spectrom. Ion Proc.* **1984**, *56*, 1–9; Grosshans, P. B.; Marshall, A. G. *Int. J. Mass Spectrom. Ion Proc.* **1990**, *100*, 347–379.
11. McIver, R. T. Jr.; Hunter, R. L.; Baykut, G. *Anal. Chem.* **1989**, *61*, 489–491.
12. McIver, R. T.; Baykut, G.; Hunter, R. L. *Int. J. Mass Spectrom. Ion Processes* **1989**, *89*, 343–358.
13. Marshall, A. G.; Wang, T. L.; Ricca, T. L. *J. Am. Chem. Soc.* **1985**, *107*, 7893–7897.
14. Wang, T. L.; Ricca, T. L.; Marshall, A. G. *Anal. Chem.* **1986**, *58*, 2935–2938.
15. Comisarow, M. B. *J. Chem. Phys.* **1978**, *69*, 4097–4104.
16. Hunter, R. L.; Sherman, M. G.; McIver, R. T. Jr. *Int. J. Mass Spectrom. Ion Proc.* **1983**, *50*, 259–274; Lee, S. H.; Wanczek, K. P.; Hartman, H. *Adv. Mass Spectrom.* **1980**, *88*, 1645–1649.
17. Wang, M.; Marshall, A.G. *Anal. Chem.* **1989**, *61*, 1288–1293.